Investigating the Tetragonal-to-Orthorhombic Phase Transition of Methylammonium Lead Iodide Single Crystals by Detailed Photoluminescence Analysis

Konstantin Schötz, Abdelrahman M. Askar, Anna Köhler, Karthik Shankar, and Fabian Panzer*

Here, the phase-transition from tetragonal to orthorhombic crystal structure of the halide perovskite methylammonium lead iodide single crystal is investigated. Temperature dependent photoluminescence (PL) measurements in the temperature range between 165 and 100 K show complex PL spectra where in total five different PL peaks can be identified. All observed PL features can be assigned to different optical effects from the two crystal phases using detailed PL analyses. This allows to quantify the fraction of tetragonal phase that still occurs below the phase transition temperature. It is found that at 150 K, 0.015% tetragonal phase remain, and PL signatures are observed from quantum confined tetragonal domains, suggesting their size to be about 7–15 nm down to 120 K. The tetragonal inclusions also exhibit an increased Urbach Energy, implying a high degree of structural disorder. The results first illustrate how a careful analysis of the PL can serve to deduce structural information, and second, how structural deviations in halide perovskites have a significant impact on the optoelectronic properties of this promising class of semiconductors.

1. Introduction

The unique development of optoelectronic components based on halide perovskites has attracted much attention in recent

K. Schötz, Prof. A. Köhler, Dr. F. Panzer
Soft Matter Optoelectronics
University of Bayreuth
Bayreuth 95440, Germany
E-mail: fabian.panzer@uni-bayreuth.de
A. M. Askar, Prof. K. Shankar
Department of Electrical and Computer Engineering
University of Alberta
Edmonton, AB T6G 1H9, Canada
Prof. A. Köhler
Bayreuth Institute of Macromolecular Research (BIMF) and Bavarian
Polymer Institute (BPI)
University of Bayreuth
Bayreuth 95440, Germany

The ORCID identification number(s) for the author(s) of this article can be found under https://doi.org/10.1002/adom.202000455.

years. In addition to the development of suitable film production methods, progress in understanding the relationship between the perovskite crystal structure and electronic structure, i.e., optical properties, is an important building block for their success.[1–3] In this context, the prototypical halide perovskite $MAPbI_3$ has developed as model system, as it also exhibits a temperature induced phase transition between tetragonal and orthorhombic crystal structure at around 160 K, which clearly affects its optical properties.[4–7] Various parameters have been identified which can influence this phase transition, such as the exact stoichiometry of the perovskite[8] or external constraints.[9] Also, the phase transition was found to proceed differently with temperature, depending on whether a single crystal or a thin film is investigated. In the case of thin films, aspects such as strain, disorder or polycrystallinity were reported to play an important role in inhibiting the phase transition, i.e., it takes place at lower temperatures and/or over a wider temperature range.[10] Accordingly, the existence of tetragonal phase even far below 160 K was reported, mostly based on temperature-dependent optical investigations.[4,11,12] In contrast, studies on single crystals, often based on scattering investigations, suggest that the phase transition is complete at higher temperatures, i.e., it proceeds in a small temperature range of a few Kelvin.[13,14] In contrast to scattering methods, the investigation of the phase transition by temperature-dependent optical spectroscopy is relatively easily accessible. It exploits the fact that tetragonal and orthorhombic phases have different band gaps and thus exhibit distinct optical signatures. However, several additional peaks and/or shoulders are often observed in the photoluminescence (PL) spectra during the transition and at lower temperatures for single crystals.[4,13,15] The exact origin of these additional PL signatures is still under debate and thus no precise understanding of the phase transition has evolved yet. In general, it has been shown that self-absorption effects can play an important role and need to be considered when analyzing measured PL spectra.[16–22] We recently demonstrated that self-absorption can even lead to additional peaks in measured PL. With a relatively simple optical model it was possible to reproduce and
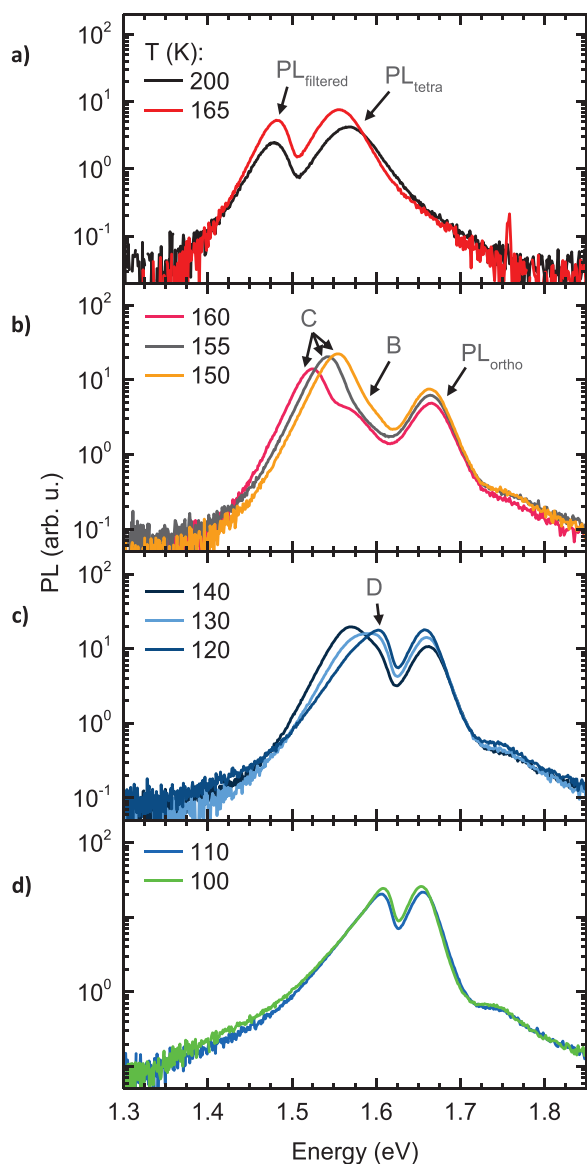
Figure 1. a–d) Temperature-dependent photoluminescence of a MAPbI$_3$ single crystal from 200 to 100 K, grouped in different temperature regions.

analyze the additional peaks in the case of pure tetragonal or orthorhombic crystal phases.[23]

Encouraged by these findings, we investigate in detail the tetragonal-orthorhombic phase transition of a MAPbI$_3$ single crystal using temperature-dependent PL spectroscopy. In the temperature range from 160 to 100 K, we observe complex PL spectra with five different PL peaks. By systematic investigation and detailed modelling of optical effects, it is possible to differentiate the PL signatures of electronic states from those caused by optical effects. This allows quantifying the fraction of tetragonal phase with a high sensitivity, where we find residual tetragonal phase to be present down to 120 K even in the case of a single crystal. Our work thus emphasizes the limited phase purity upon structural changes of hybrid perovskites even in the case of single crystals and sheds further light on how to analyze and interpret PL spectra consisting of multiple peaks.

2. Results

Figure 1 shows the temperature dependent PL spectra of a MAPbI$_3$ single crystal in the temperature range between 200 and 100 K, grouped into temperature ranges comprising similar spectra. The temperature for the tetragonal to orthorhombic phase transition was identified to be at 163 K in the case of single crystals.[24,25] Thus, the spectra in Figure 1a at 200 and 165 K are associated with the tetragonal phase. They show two peaks centered at about 1.55 and 1.48 eV. In a previous study we could clarify the origin of the two peaks,[23] where the higher energy peak (PL$_{tetra}$) at 1.55 eV is due to PL that leaves the crystal without significant self-absorption, such as PL generated close to the crystal surface. In contrast, the lower energy peak at 1.48 eV (PL$_{filtered}$) results from an inner filter effect, i.e., it is due to PL that suffered significant self-absorption as it experienced a longer optical path through the perovskite bulk. Here the relatively high probability for reflections at the inner surfaces of the crystal can significantly boost the length of the optical path that the filtered PL experiences (also see Figure S1 in the Supporting Information for details).

Upon further cooling, the PL spectra become more complex. In the range from 160 to 150 K, a new peak appears at 1.67 eV that shifts by about 5 meV to lower energies during cooling to 150 K. Furthermore, there is a shoulder ("peak B") around 1.57 eV at 160 K that becomes weaker with cooling, and a peak at 1.53 eV ("peak C") that shifts by 30 meV to higher energies and increases in intensity by about 60%. We can readily assign the peak at 1.67 eV to an optical transition in the orthorhombic phase (PL$_{ortho}$).[26–28] In contrast, the origin of peaks B and C is not as straightforward and needs more detailed investigation. Upon further cooling (Figure 1b), peaks B and C seem to merge, and in the temperature range from 140 to 120 K (Figure 1c), a new sharp peak at 1.60 eV appears and gains intensity (peak D). At 110 and 100 K, (lowest temperature we investigated), only PL$_{ortho}$ and peak D remain (Figure 1d). We always observed the above-described PL evolution for different MAPbI$_3$ single crystals, suggesting that it is a general behavior.

To identify the origin of the various peaks, we take a twofold approach. First, we consider PL spectra collected from a different angle. This allows us to identify self-absorption effects, as we found the relative intensity of PL$_{filter}$ to be sensitive on the measurement geometry.[23] Second, we model the optical spectra under consideration of optical effects such as reflection and reabsorption.

Figure 2a shows the PL spectra taken at 160 K for two measurement geometries, which slightly differ in the angles between single crystal and the incident laser beam. The difference between the two spectra is also shown (orange shaded area). It is obvious that the spectra differ only in the intensity of peak C, indicating that peak C stems from filtered PL due to self-absorption effects. Likewise, the PL spectra taken under varied geometries at 100 K (Figure 2b) differ in the intensity of peak D, so that we assign peak D to filtered PL of the orthorhombic phase (see Figure S2 in the Supporting Information for all measured spectra between 165 and 100 K).

To underpin the assignment of peak C and peak D to filtered PL, we attempt to reproduce the spectra by optical modelling as
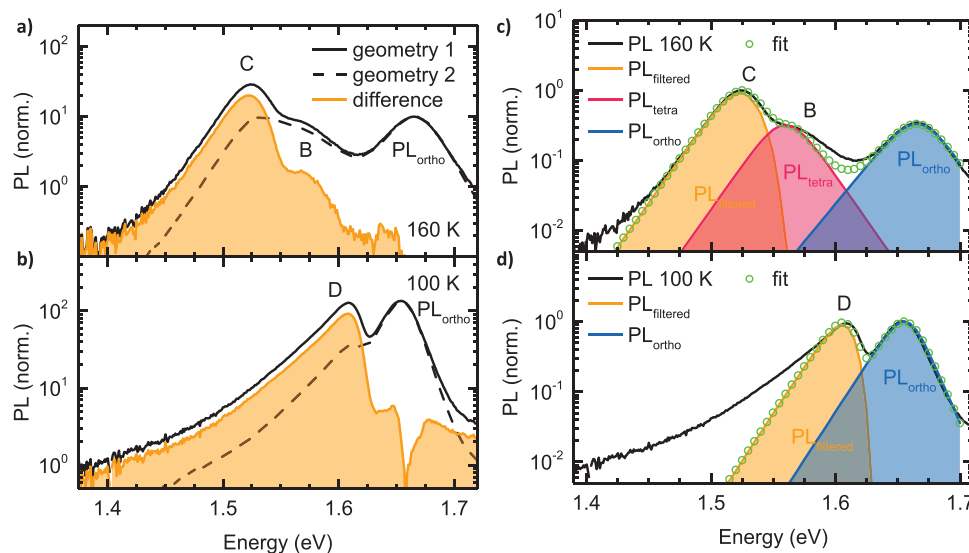
Figure 2. a,b) PL of a MAPbI$_3$ single crystal in a geometry with strongly (black solid) and weakly pronounced (black dashed) self-absorption effect, as well as the difference (orange) between both spectra at a) 160 K and b) 100 K. c,d) Modelled PL (green circles) considering self-absorption, decomposed in tetragonal (red), orthorhombic (blue), and filtered PL (orange) at c) 160 K and d) 100 K, together with the measured PL spectra (black solid lines).

presented in our earlier work.[23] In brief, we consider the one dimensional charge carrier distribution generated in the crystal by our 337 nm laser excitation. This charge carrier distribution leads to PL that can travel either to the front or to the back of the crystal, where it is transmitted or reflected at the interface of the perovskite and its surrounding media. The probability for this is determined by the refractive index of the perovskite and the surrounding media, in our case helium. On the way through the crystal, the PL is absorbed by the perovskite. Considering a possible mismatch of excitation and detection spot, the PL leaving the crystal after multiple reflections (filtered PL) can be amplified by a constant factor in our model. The crystal length is set to 1 mm, in accordance with the size of the used crystal. The reflection probability at the perovskite-helium interface is estimated to be 0.85 by using the Fresnel equations and averaging over all incident angles. For the absorption spectra of the tetragonal phase of MAPbI$_3$, we combine the room temperature absorption coefficient reported by Crothers et al.[29] with the temperature-dependent absorbance data of the Urbach tail reported by Ledinsky et al.[30] Since during the phase transition tetragonal and orthorhombic phase coexist, the total absorption spectrum of the crystal is a combination of a certain fraction of tetragonal phase absorption and orthorhombic phase absorption. For the latter, the absorption coefficient is approximated by absorption data from thin films and an extrapolated Urbach tail based on transmission measurements of a single crystal (see Section S3 in the Supporting Information for full details of the modelling approach).[6,23] In principle, and similar to absorption, the total PL spectrum is the sum of tetragonal and orthorhombic PL. Since energy transfer from the orthorhombic to the energetically lower tetragonal phase can occur easily,[31,32] the tetragonal PL is expected to appear over-proportionally intense in the measured spectra. Furthermore, the different PL features, including filtered PL and the intrinsic PL peaks of tetragonal and orthorhombic phases, typically overlap spectrally. This makes the modeling of the measured

spectra in the phase transition region more complex compared to the analyses of PL spectra of pure phases. A complete modeling of the spectra, including a clear identification of peak C and D, requires first to identify clearly the contributions from neat phases. To access the spectral shape of the intrinsic PL, we recall that the PL lineshape as a function of photon energy E of a classic inorganic semiconductor is described by a generalized Planck law, which reads

$$\mathrm{PL}(E) \propto A(E)E^2 \exp\left(-\frac{E}{k_B T}\right) \qquad (1)$$

where $A(E)$ is the absorptivity, k_B is the Boltzmann constant and T is the temperature.[33] For the intrinsic PL line-shape, i.e., the PL without effects of self-absorption, $A(E)$ in Equation (1) can be replaced by the absorption coefficient $\alpha(E)$ (see Section S4 in the Supporting Information).[34] Below the band gap, MAPbI$_3$ shows band tail absorption, which decreases exponentially toward lower energies.[35] It is well described by Urbach tail absorption, expressed by $\alpha(E < E_g) \propto \exp(E/E_u)$, with E_u being the Urbach Energy.[36] Above the band gap, the absorption is roughly constant in the relevant energy range for the PL, that is the spectral range where PL and absorption overlap (Figure S3, Supporting Information). We thus approximate the shape of the absorption spectrum according to

$$\alpha(E) \approx \frac{\alpha_0}{\exp\left(-\frac{E - E_0}{E_u}\right) + 1} \qquad (2)$$

(see Section S4 and Figure S3 in the Supporting Information for details regarding comparison of modelled and experimental spectra). The PL lineshape is then given by

$$\mathrm{PL}(E) \approx I_0 \frac{1}{\exp\left(-\frac{E - E_0}{E_u}\right) + 1} E^2 \exp\left(-\frac{E}{k_B T}\right) \qquad (3)$$

Using Equation (3), we fitted PL data of MAPbI$_3$ single crystals and thin film at different temperatures where the material is either in the pure tetragonal or pure orthorhombic phase. We obtained a good agreement between experimental and fitted PL (Figures S3 and S4, Supporting Information), although it was necessary to replace $\exp(-E/k_BT)$ with $\exp(-0.825E/k_BT)$ in Equation (3) in the case of single crystals. While the origin of this factor is not fully clear, there are indications that it occurs from a self-absorption effect as described in more detail in the Supporting Information (Section S5, Supporting Information).

Successfully modelling the intrinsic PL spectra of pure crystal phases builds the basis for modeling and fitting the measured PL at 160 K, where tetragonal and orthorhombic phases coexist. While the temperature is given from the experimental conditions, the relative intensities and energetic positions of the intrinsic PL peaks, the Urbach energies and the fraction of tetragonal inclusions are optimized to obtain best agreement with the measured spectrum. We use the energetic position of the tetragonal PL peak at 165 K, assuming that it does not change significantly within the first 5 K of the phase transition. The modelled PL with its decomposition in the individual contributions is depicted in Figure 2c, showing very good agreement with the experimental data. This underpins that peak C is due to filtered PL, while peak B appears to stem from residual tetragonal inclusions. At 100 K, we model the PL assuming that tetragonal inclusions are absent (Figure 2d). The modelled PL can nicely reproduce peak D, further supporting that it is due to filtered PL from the orthorhombic phase. However, the low energy edge, i.e., the PL below ≈1.56 eV, cannot be reproduced assuming only orthorhombic PL.

Having understood the individual features in the PL spectrum at 160 K, we next attempt to extract detailed information about the tetragonal-orthorhombic phase transition by fitting the measured PL spectra between 160 and 100 K using our modelling approach. To do so, it is reasonable to investigate how a variation of parameters such as the content of tetragonal inclusions, the tetragonal PL intensity or tetragonal PL peak position affects the modelled spectra. **Figure 3**a shows modelled PL spectra differing in the content of tetragonal inclusions, while all other parameters remained unchanged. Upon reducing the content of tetragonal inclusions from 1% to 0.1%, peak C shifts from ≈1.52 to ≈1.55 eV and its intensity increases. This PL change follows since the reduction of the content of tetragonal phase is accompanied by a corresponding change in the absorption edge, thus influencing the effect of self-absorption on the intrinsic PL. This causes the signature of the filtered PL to shift more and more toward the spectral position of the intrinsic PL of the tetragonal phase. These spectral changes fit nicely to the measured PL changes between 160 and 150 K in Figure 1b. Here we also want to point out that the above-mentioned relationship between the fraction of tetragonal phase and the energetic spacing between PL$_{tet,filter}$ and PL$_{tet,intrinsic}$ allows extracting the fraction of tetragonal phase from fitting our model to the measured PL spectra. Upon cooling, the experimentally observed shift of peak C saturates at 1.57 eV (Figure 1b), where it becomes indistinguishable from PL$_{tetra}$, similar to the spectral changes in the modelled spectra for a decreasing fraction of tetragonal phase below 0.1% (Figure 3a). Further reducing the fraction of tetragonal phase results in an enhancement
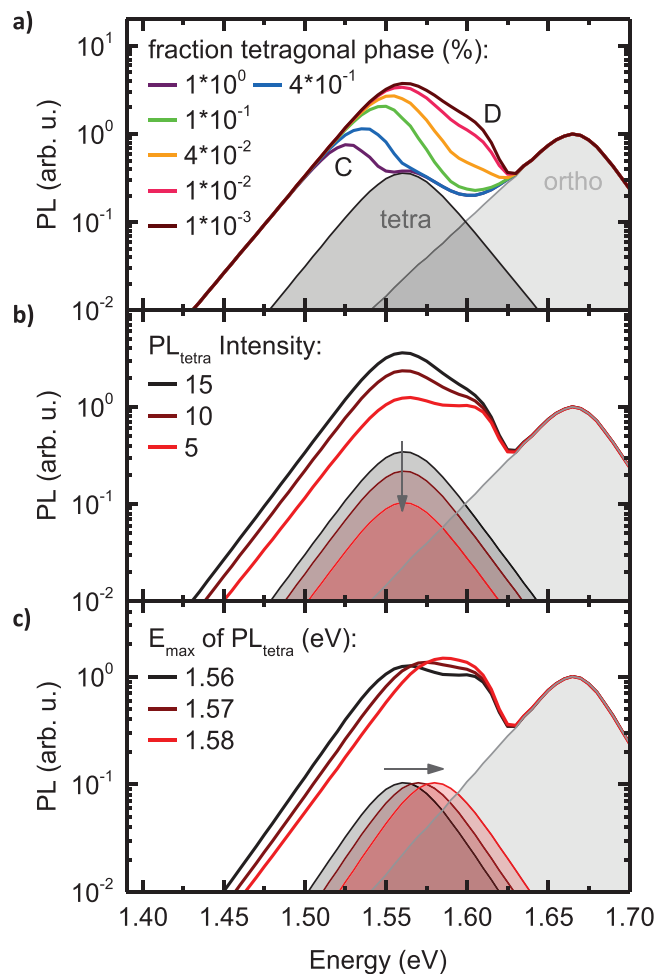

Figure 3. Modeled PL for a) different fractions of tetragonal phase, b) decreasing tetragonal PL intensities, and c) blue-shift of the tetragonal PL peak, using the spectral shapes of tetragonal and orthorhombic PL at 160 K.

of a PL signal at ≈1.6 eV. This is caused by the fact that the small fraction of tetragonal phase has only little influence on the absorption edge, which is thus almost exclusively dominated by absorption of the orthorhombic phase. Accordingly, the self-absorption effect is mainly determined by the absorption of the orthorhombic phase, i.e., the feature at 1.6 eV corresponds to filtered PL of the orthorhombic phase. The peak position of this PL feature, as well as its growth, fit very well with the experimentally observed appearance of peak D between 140 and 120 K in Figure 1c. So far, we can conclude that the shift of peak C and the emergence of peak D observed in the measurements upon cooling from 160 to 120 K can be understood qualitatively simply as the result of a reduction in the fraction of tetragonal phase. However, from Figure 1b it becomes clear that upon cooling the low energy edge (<1.5 eV) of the measured PL spectra shifts to higher energies, a spectral dynamic which cannot be captured by just changing the content of tetragonal phase in our model (Figure 3a). This makes it necessary to also allow changing the PL intensity of the tetragonal phase, which is reasonable as the fraction of tetragonal phase decreases. The impact of changing the PL$_{tetra}$ intensity on the overall PL

ADVANCED
SCIENCE NEWS
www.advancedsciencenews.com

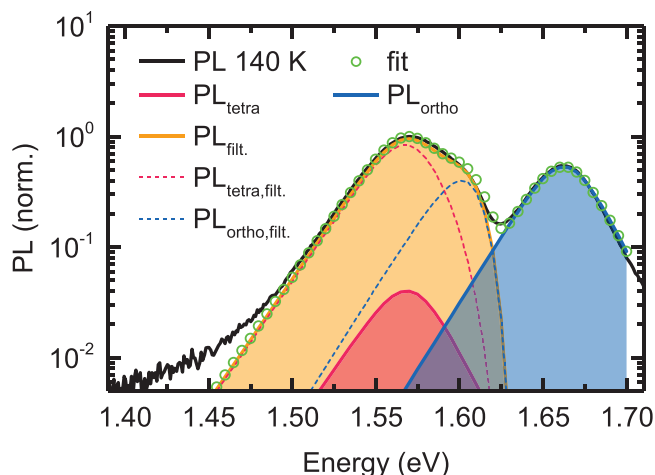ADVANCED
OPTICAL
MATERIALS
www.advopticalmat.de

Figure 4. Measured (black solid line) and modelled (green circles) PL at 140 K and spectral decomposition in orthorhombic (blue), tetragonal (red), and filtered PL (orange). The dashed lines indicate individual contributions of orthorhombic and tetragonal phase to the filtered PL.

Figure 5. a) Intensity of the tetragonal PL normalized to the value at 165 K (black squares) together with the content of tetragonal phase in the crystal (orange circles) as a function of temperature. The content of tetragonal phase at 155 and 150 K as extracted from transmission measurements on similar MAPbI$_3$ single crystals from an earlier work[23] is also shown (open black circles). The grey shaded area indicates the upper limit of the content of tetragonal phase below 140 K. b) Temperature-dependence of the tetragonal PL peak position. c) Temperature dependent Urbach energies of the tetragonal (blue triangles) and orthorhombic phase (green squares) together with fits according to Equation (5).

spectrum is shown in Figure 3b, where exemplarily PL$_{tetra}$ is reduced to a third of its intensity, while the fraction of tetragonal phase is constant at 0.001%. With that, it is possible to account for the experimentally observed shift of the low energy edge, while it is also obvious, that lowering the tetragonal PL intensity always results in a double peak in the spectral region between 1.50 and 1.60 eV, consisting of peak C/B and peak D. This is at variance especially with the measured PL spectrum at 130 K (Figure 1c), where we observed only one broadened peak in the energy range between 1.50–1.63 eV. Allowing PL$_{tetra}$ to shift to higher energies by about 20 meV resolves this deviation between modelled and experimental PL (see Figure 3c).

Using the insights gained from Figure 3, we finally modelled the measured spectra between 160 and 100 K. To fit the measured spectra we varied the fraction of tetragonal phase, PL$_{tetra}$ peak position and PL$_{tetra}$ intensity. Furthermore from modeling the intrinsic PL of tetragonal and orthorhombic phase using Equation (3), also the Urbach energies of the two phases $E_{u,tetra}$ and $E_{u,ortho}$, were derived. **Figure 4** shows an exemplary fit and its spectral decomposition for the PL at 140 K, (see Figure S5 in the Supporting Information for fits to the PL spectra at the other temperatures investigated), from which the good match between measured spectrum and modelled PL is evident. From Figure 4, it also becomes clear how significant the proportion of filtered PL from the tetragonal phase (red dashed line in Figure 4) can be, even though the intensity of the intrinsic PL$_{tetra}$ (solid red line in Figure 4) is relatively low.

Fitting the temperature dependent PL spectra yields the temperature evolution of the fit parameters. **Figure 5**a shows the content of tetragonal inclusions and the integrated intensity of the direct tetragonal PL (normalized to the value at 165 K) between 165 and 100 K. We also extracted the content of tetragonal inclusions based on transmission data of a MAPbI$_3$ single crystal from one of our earlier works.[23] This crystal was grown via the same synthesis route as the crystal used in this study, so that we expect a similar phase transition behavior. Indeed, we find that the content of tetragonal inclusions extracted from
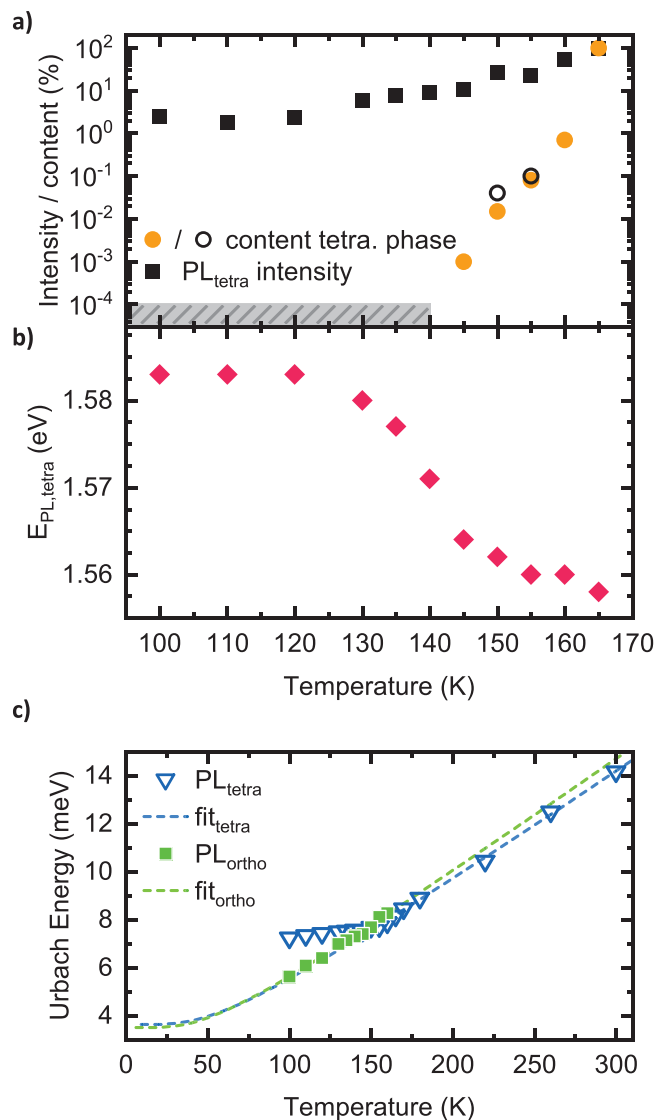
both methods (transmission and PL measurements) agree well, supporting our PL analysis approach. Upon cooling, the content of tetragonal phase drops drastically from 100% at 165 K to 0.7% at 160 K. From there, it further decreases exponentially by about two decades per ten Kelvin to 0.001% at 145 K. At 140 K, the content is so low that no PL filter-effect of tetragonal inclusions occurs, so that a precise quantification of the fraction of tetragonal phase is not possible anymore. Nevertheless, the missing filter effect allows estimating the content of tetragonal inclusions to be below 10^{-4}% (indicated as grey shaded area

2000455 (5 of 9)

ADVANCED
SCIENCE NEWS
www.advancedsciencenews.com

ADVANCED
OPTICAL
MATERIALS
www.advopticalmat.de

in Figure 5a). Similarly, the integrated intensity of the direct tetragonal PL decreases roughly exponentially upon cooling, reaching 2% at 120 K. Thus, it decreases at a rate of about 0.4 decades per ten Kelvin, i.e., less drastic than the decrease of content of tetragonal inclusions. From 120 K, the intensity of the direct tetragonal PL stays roughly constant. However, as mentioned before, below 120 K the spectral signatures of the tetragonal phase is very weak, so that corresponding fit parameters might exhibit a relatively large error. From the temperature dependent fitting of the measured PL spectra, also the peak position of the tetragonal PL was extracted, which is shown in Figure 5b. Starting from 1.558 eV at 165 K, the PL shifts to higher energies, i.e., to 1.562 eV at 150 K. Upon further cooling, this shift becomes more intense, so that the peak position of PL_{tetra} is 1.580 eV at 130 K. After that it reaches its final position at 1.583 eV at 120 K. Figure 5c displays the temperature-dependence of the Urbach energies of the tetragonal and the orthorhombic phase $E_{u,tetra}$ and $E_{u,ortho}$. Here we assume that the factor of 0.825 that we needed to introduced in Equation (3) (*vide supra*) has an artificial origin. We therefore corrected the Urbach energies obtained by fitting Equation (3) to the PL data accordingly (see Section S5 in the Supporting Information). The Urbach energy of the pure tetragonal phase decreases linearly from 14.2 meV at 300 K to 8.2 meV at 165 K. In the temperature range of the phase transition, this trend continues until 155 K, where the Urbach energy of the tetragonal phase is 7.7 meV. Upon further cooling, the decrease in $E_{u,tetra}$ flattens out, changing by only 0.5 meV from 155 to 100 K. At 160 K $E_{u,ortho}$ is 8.2 meV, i.e., similar to the value of $E_{u,tetra}$ at this temperature. However in contrast to the behavior of $E_{u,tetra}$ in the transition region, $E_{u,ortho}$ decreases more rapidly, that is, with a similar slope as $E_{u,tetra}$ between 300 and 165 K, reaching a value of 5.6 meV at 100 K (Figure 5c). The temperature-dependence of the Urbach energy can be expressed as[37]

$$E_u(T) = \left(\frac{\Theta}{\sigma_0}\right)\left[\frac{1+X}{2} + \left\{\exp\left(\frac{\Theta}{T}\right) - 1\right\}^{-1}\right] \tag{4}$$

where T is the absolute temperature, θ is the Einstein characteristic temperature of the phonons that interact with the free charges,[37,38] and σ_0 is the so-called Urbach Edge parameter.[37] The parameter $X = \langle U^2 \rangle_x / \langle U^2 \rangle_0$, with $\langle U^2 \rangle_0$ being the zero-point uncertainty of the atomic positions, is related to the structural disorder in the system and would be zero for a perfect crystal.[37,39] Assuming a perfect crystal ($X = 0$), the term $\theta/(2\sigma_0)$ can be referred to as the static disorder $E_{u,0}$, and Equation (4) becomes[40]

$$E_u(T) = E_{u,0} + 2E_{u,0} \cdot \left\{\exp\left(\frac{\Theta}{T}\right) - 1\right\}^{-1} \tag{5}$$

Fitting Equation (5) to the temperature dependent Urbach energies of the orthorhombic phase from Figure 5c yields $E_{u,0,ortho} = (3.5 \pm 0.3)$ meV and $\theta_{ortho} = (145 \pm 13)$ K. For the pure tetragonal phase, (i.e., considering the Urbach energies between 300 and 165 K), we obtain $E_{u,0,tetra} = (3.6 \pm 0.4)$ meV and $\theta_{tetra} = (156 \pm 19)$ K. Within the accuracy of the approach, these values are identical to the values of the orthorhombic

phase. The fits are indicated as dashed lines in Figure 5d. In case of the tetragonal phase below the phase transition temperature, a clear deviation between the expected Urbach energies from Equation (5) and the values obtained from the measured PL spectra becomes obvious.

3. Discussion

Several studies have so far investigated the tetragonal to orthorhombic phase transition of $MAPbI_3$ thin films, powder and single crystals. For thin films, typically a large temperature range of 20–40 K can be observed in which both phases coexist.[4,10,12,41,42] This is argued to be caused by the polycrystalline nature of those films, where every grain can have a slightly different transition temperature, depending, e.g., on the grain size,[43] or the strain induced by the substrate.[10,11,44] In powders, the temperature range of the coexistence was reported to be smaller with 5–12 K,[10,45] which is likely due to the absence of substrate-induced stress on the lose particles.[10,46] For single crystals, older works suggested that the tetragonal-to-orthorhombic phase transition is abrupt and that there is no coexistence of the two phases.[13,15] However, more recent works suggest that there is a small temperature window, in which such a coexistence can be observed. Our finding that the fraction of tetragonal phase reduces rapidly by ≈99% within the first 5 K of the transition (Figure 5a), thus is in line with the observations found in literature. However, the fact that we observe PL signatures of tetragonal inclusions down to at least 120 K deviates from the expectations from literature. This finding suggests that also in the case of single crystals, certain structural states in halide perovskites persist even if external parameters such as temperature are changed over a wide range. In contrast to the rapid decrease of the fraction of tetragonal phase below the phase transition, the change in PL intensity of the tetragonal inclusions shows a considerably milder decrease (Figure 5a). This implies an efficient energy transfer from orthorhombic phase to the tetragonal inclusions in the temperature range of the phase transition, which is in line with literature reports.[31,32] It also suggests that the tetragonal inclusions can act as highly efficient traps for the excited states of the predominant orthorhombic perovskite phase.

We also observed and quantified a blue shift of the PL of the tetragonal inclusions by about 20 meV between 155 and 120 K (Figure 5b). One cause of such a shift could be strain on the tetragonal inclusions due to a mismatch between the lattice constants of tetragonal and orthorhombic phase.[47] Based on temperature-dependent PL measurements and comparison with associated lattice constants, it is possible to estimate the strain that would be necessary to shift the PL by 20 meV to higher energies via the Birch-Murnaghan-equation.[48] With the assumption that lattice dilation is the dominant factor for the temperature-dependent shift of the PL maximum,[6,12] we find tensile strain values of 85–165 MPa (see Section S7 in the Supporting Information for details). However, recent studies demonstrated that the unit cell volume of the orthorhombic phase is smaller than the one of the tetragonal phase,[4,45,49,50] and thus there should be compressive strain instead of tensile strain to affect the tetragonal inclusions. Room temperature measurements showed that

pressure on MAPbI$_3$ leads to a red shift.[51–54] Assuming this to also hold true at lower temperatures, strain would not be a satisfying explanation of the observed blue shift.

An alternative interpretation of the blue-shift is via a quantum confinement effect, where the decreasing domain size confines the excited state, leading to a blue-shift of the PL.[55] The observed blue-shift of 20 meV implies domain sizes of 7–15 nm, based on the correlation between PL peak position and crystal size of MAPbI$_3$ nanocrystals found in literature,[56–58] and on the assumption that this correlation also applies to the tetragonal inclusions. We estimate the domain volume to be about $(15\ \text{nm})^3$, consider that 0.001% of the crystal is in the tetragonal phase (as it is the case at 145 K) and we assume that the tetragonal inclusions are distributed homogeneously. From this, we obtain a number concentration of $3 \times 10^{12}\ \text{cm}^{-3}$ and an average distance of about 0.7 µm between the tetragonal inclusions. This is in the range of the charge carrier diffusion length reported in literature,[59,60] suggesting that an efficient energy transfer from orthorhombic phase to the tetragonal inclusions is well possible. This also fits well with our observation that the fraction of tetragonal phase decreases more rapidly compared to the corresponding PL intensity (Figure 5a). These results also emphasize that due to the efficient energy transfer, even a low density of domains that deviate regarding their structure from the investigated perovskite can have significant impact on its PL spectra and thus its photophysical properties.

Regarding the extracted temperature dependent Urbach energies of both phases, we find that the values of $E_{u,0,tetra}$ and θ_{tetra} agree well with the results from Ledinsky et al.,[40] who quantified the temperature dependent Urbach Energies of the tetragonal phase of MAPbI$_3$ thin films also on the basis of PL measurements. Also, our observation that θ_{tetra} and θ_{ortho} exhibit identical values indicates, that the electronically active phonon modes are the same for orthorhombic and tetragonal phase and that their energy does not change upon the phase transition. Further, we observed that during the coexistence of both phases, the extracted values for $E_{u,tetra}$ deviate from the ones expected according to Equation (5). Since θ appears to be constant, the higher values of $E_{u,tetra}$ indicate a higher static disorder in the tetragonal inclusions, increasing with decreasing domain size. This is reasonable, when considering that the orthorhombic and the tetragonal unit cells have different lattice constants,[4] implying the build-up of strain in the tetragonal inclusions (see above). The strain leads to a distorted crystal structure, so that X (being a measure for the static disorder) in Equation (4) increases.

Finally, we note that the PL in the temperature range from 160 to 120 K can be modelled with tetragonal, orthorhombic and the corresponding filtered PL and no additional peaks are necessary. This suggests in particular that there is no significant contribution of bound excitons and defects to the PL spectra down to 120 K.

4. Conclusion

In summary, we investigated the tetragonal-to-orthorhombic phase transition of MAPbI$_3$ single crystals using temperature dependent PL measurements. We carefully considered and modelled optical effects to distinguish between optical features

and intrinsic electronic transitions in measured PL spectra. We quantified the fraction of tetragonal phase during the transition with a high sensitivity, where we find that the tetragonal fraction at 150 K has reduced to 0.001%. Additionally, we can still identify PL signatures of tetragonal phase down to 120 K, where its spectrum shifts to higher energies, being indicative of a confinement effect of the last bit of tetragonal inclusions. Overall, this work demonstrates that the phase transition in MAPbI$_3$ single crystals is not abrupt, but extends over 40 K, and PL of bound excitons does not play a role above 100 K in our experiments. Furthermore, our results show that even smallest contents of structurally different inclusions in the perovskite can have significant impact on its opto-electronic properties. This aspect will be also relevant for perovskites with mixed stoichiometry, where the structural homogeneity and its influence on the optoelectronic properties is still unclear but crucial for the further development of highly efficient perovskite solar cells.

5. Experimental Section

Sample Preparation: MAPbI$_3$ single crystals were prepared following the inverse temperature crystallization technique.[61] In brief, the synthesis started with a 1–1.3 M solution of MAI (from Dyesol-Limited, Now GreatCell Solar) and PbI$_2$ (Sigma-Aldrich) in gamma-Butyrolactone (GBL, Sigma-Aldrich). The precursors dissolved in GBL after 30 min of vigorous stirring at 60 °C. Upon filtering the solution using 0.22 µm PVDF filters, the stock solution was then distributed into small vials with 3–4 mL of solution each. The vials were kept undisturbed in an oil bath for 34 h at 110 °C. Once the desired size of the crystals was achieved, the crystals were removed from the synthesis solution, washed quickly with fresh GBL, dried with a N$_2$ flow.

Photoluminescence Measurements: The temperature-dependent PL measurements were performed using a home-built setup. The sample was put in a continuous flow cryostat (Oxford Instruments, Optistat CF) with an automated temperature controller (Oxford Instruments ITC503S). The sample was excited with a 337 nm nitrogen laser (LTB MNL 100). The signal was collected via a charge-coupled device (CCD) camera (Andor iDus DU420a-OE) coupled to a spectrograph (Andor Shamrock SR303i).

Supporting Information

Supporting Information is available from the Wiley Online Library or from the author.

Acknowledgements

Conflict of Interest

The authors declare no conflict of interest.

[1] L. M. Herz, *Annu. Rev. Phys. Chem.* **2016**, *67*, 65.

[2] Y. Kanemitsu, *J. Mater. Chem. C* **2017**, *5*, 3427.

[3] D. W. deQuilettes, K. Frohna, D. Emin, T. Kirchartz, V. Bulovic, D. S. Ginger, S. D. Stranks, *Chem. Rev.* **2019**, *119*, 11007.

[4] W. Kong, Z. Ye, Z. Qi, B. Zhang, M. Wang, A. Rahimi-Iman, H. Wu, *Phys. Chem. Chem. Phys.* **2015**, *17*, 16405.

[5] A. Glushkova, K. Mantulnikovs, G. Giriat, K. Semeniuk, L. Forro, E. Horvath, A. Arakcheeva, *Sol. RRL* **2019**, *3*, 1900044.

[6] S. Singh, C. Li, F. Panzer, K. L. Narasimhan, A. Graeser, T. P. Gujar, A. Köhler, M. Thelakkat, S. Huettner, D. Kabra, *J. Phys. Chem. Lett.* **2016**, *7*, 3014.

[7] E. S. Parrott, R. L. Milot, T. Stergiopoulos, H. J. Snaith, M. B. Johnston, L. M. Herz, *J. Phys. Chem. Lett.* **2016**, *7*, 1321.

[8] T. Meier, T. P. Gujar, A. Schönleber, S. Olthof, K. Meerholz, S. van Smaalen, F. Panzer, M. Thelakkat, A. Köhler, *J. Mater. Chem. C* **2018**, *6*, 7512.

[9] N. Arad-Vosk, N. Rozenfeld, R. Gonzalez-Rodriguez, J. L. Coffer, A. Sa'ar, *Phys. Rev. B* **2017**, *95*, 085433.

[10] A. Osherov, E. M. Hutter, K. Galkowski, R. Brenes, D. K. Maude, R. J. Nicholas, P. Plochocka, V. Bulović, T. J. Savenije, S. D. Stranks, *Adv. Mater.* **2016**, *28*, 10757.

[11] C. Wehrenfennig, M. Z. Liu, H. J. Snaith, M. B. Johnston, L. M. Herz, *APL Mater.* **2014**, *2*, 081513.

[12] F. Panzer, C. Li, T. Meier, A. Köhler, S. Huettner, *Adv. Energy Mater.* **2017**, *7*, 1700286.

[13] H. H. Fang, R. Raissa, M. Abdu-Aguye, S. Adjokatse, G. R. Blake, J. Even, M. A. Loi, *Adv. Funct. Mater.* **2015**, *25*, 2378.

[14] G. Schuck, D. M. Tobbens, M. Koch-Muller, I. Efthimiopoulos, S. Schorr, *J. Phys. Chem. C* **2018**, *122*, 5227.

[15] L. Q. Phuong, Y. Nakaike, A. Wakamiya, Y. Kanemitsu, *J. Phys. Chem. Lett.* **2016**, *7*, 4905.

[16] M. Chauhan, Y. Zhong, K. Schötz, B. Tripathi, A. Köhler, S. Huettner, F. Panzer, *J. Mater. Chem. A* **2020**, *8*, 5086.

[17] L. M. Pazos-Outón, M. Szumilo, R. Lamboll, J. M. Richter, M. Crespo-Quesada, M. Abdi-Jalebi, H. J. Beeson, M. Vrućinić, M. Alsari, H. J. Snaith, B. Ehrler, R. H. Friend, F. Deschler, *Science* **2016**, *351*, 1430.

[18] Y. J. Fang, H. T. Wei, Q. F. Dong, J. S. Huang, *Nat. Commun.* **2017**, *8*, 14417.

[19] Y. Yamada, T. Yamada, L. Q. Phuong, N. Maruyama, H. Nishimura, A. Wakamiya, Y. Murata, Y. Kanemitsu, *J. Am. Chem. Soc.* **2015**, *137*, 10456.

[20] T. Yamada, Y. Yamada, H. Nishimura, Y. Nakaike, A. Wakamiya, Y. Murata, Y. Kanemitsu, *Adv. Electron. Mater.* **2016**, *2*, 1500290.

[21] F. Staub, I. Anusca, D. C. Lupascu, U. Rau, T. Kirchartz, *J. Phys.: Mater.* **2020**, *3*, 025003.

[22] D. C. Hong, J. Li, S. S. Wan, I. G. Scheblykin, Y. X. Tian, *J. Phys. Chem. C* **2019**, *123*, 12521.

[23] K. Schötz, A. M. Askar, W. Peng, D. Seeberger, T. P. Gujar, M. Thelakkat, A. Köhler, S. Huettner, O. M. Bakr, K. Shankar, F. Panzer, *J. Mater. Chem. C* **2020**, *8*, 2289.

[24] A. Poglitsch, D. Weber, *J. Chem. Phys.* **1987**, *87*, 6373.

[25] R. E. Wasylishen, O. Knop, J. B. Macdonald, *Solid State Commun.* **1985**, *56*, 581.

[26] G. Xing, N. Mathews, S. S. Lim, N. Yantara, X. Liu, D. Sabba, M. Gratzel, S. Mhaisalkar, T. C. Sum, *Nat. Mater.* **2014**, *13*, 476.

[27] K. Wu, A. Bera, C. Ma, Y. Du, Y. Yang, L. Li, T. Wu, *Phys. Chem. Chem. Phys.* **2014**, *16*, 22476.

[28] R. L. Milot, G. E. Eperon, H. J. Snaith, M. B. Johnston, L. M. Herz, *Adv. Funct. Mater.* **2015**, *25*, 6218.

[29] T. W. Crothers, R. L. Milot, J. B. Patel, E. S. Parrott, J. Schlipf, P. Müller-Buschbaum, M. B. Johnston, L. M. Herz, *Nano Lett.* **2017**, *17*, 5782.

[30] M. Ledinsky, T. Schonfeldova, J. Holovsky, E. Aydin, Z. Hajkova, L. Landova, N. Neykova, A. Fejfar, S. De Wolf, *J. Phys. Chem. Lett.* **2019**, *10*, 1368.

[31] H. Wang, L. Whittaker-Brooks, G. R. Fleming, *J. Phys. Chem. C* **2015**, *119*, 19590.

[32] L. Q. Phuong, Y. Yamada, M. Nagai, N. Maruyama, A. Wakamiya, Y. Kanemitsu, *J. Phys. Chem.* **2016**, *7*, 2316.

[33] P. Würfel, *J. Phys. C: Solid State Phys.* **1982**, *15*, 3967.

[34] E. Daub, P. Würfel, *Phys. Rev. Lett.* **1995**, *74*, 1020.

[35] S. Pathak, A. Sepe, A. Sadhanala, F. Deschler, A. Haghighirad, N. Sakai, K. C. Goedel, S. D. Stranks, N. Noel, M. Price, S. Hüttner, N. A. Hawkins, R. H. Friend, U. Steiner, H. J. Snaith, *ACS Nano* **2015**, *9*, 2311.

[36] F. Urbach, *Phys. Rev.* **1953**, *92*, 1324.

[37] G. D. Cody, T. Tiedje, B. Abeles, T. D. Moustakas, B. Brooks, Y. Goldstein, *J. Phys. Colloq.* **1981**, *42*, C4.

[38] S. M. Wasim, C. Rincon, G. Marin, P. Bocaranda, E. Hernandez, I. Bonalde, E. Medina, *Phys. Rev. B* **2001**, *64*, 195101.

[39] M. Beaudoin, A. J. G. DeVries, S. R. Johnson, H. Laman, T. Tiedje, *Appl. Phys. Lett.* **1997**, *70*, 3540.

[40] M. Ledinsky, T. Schönfeldová, J. Holovský, E. Aydin, Z. Hájková, L. Landová, N. Neyková, A. Fejfar, S. De Wolf, *J. Phys. Chem. Lett.* **2019**, *10*, 1368.

[41] H. Tahara, M. Endo, A. Wakamiya, Y. Kanemitsu, *J. Phys. Chem. C* **2016**, *120*, 5347.

[42] V. D'Innocenzo, G. Grancini, M. J. P. Alcocer, A. R. S. Kandada, S. D. Stranks, M. M. Lee, G. Lanzani, H. J. Snaith, A. Petrozza, *Nat. Commun.* **2014**, *5*, 3586.

[43] C. Stavrakas, S. J. Zelewski, K. Frohna, E. P. Booker, K. Galkowski, K. Y. Ji, E. Ruggeri, S. Mackowski, R. Kudrawiec, P. Plochocka, S. D. Stranks, *Adv. Energy Mater.* **2019**, *9*, 1901883.

[44] Z. H. Chen, L. You, C. W. Huang, Y. J. Qi, J. L. Wang, T. Sritharan, L. Chen, *Appl. Phys. Lett.* **2010**, *96*, 252903.

[45] P. S. Whitfield, N. Herron, W. E. Guise, K. Page, Y. Q. Cheng, I. Milas, M. K. Crawford, *Sci. Rep.* **2016**, *6*, 35685.

[46] N. Leupold, K. Schötz, S. Cacovich, I. Bauer, M. Schultz, M. Daubinger, L. Kaiser, A. Rebai, J. Rousset, A. Köhler, P. Schulz, R. Moos, F. Panzer, *ACS Appl. Mater. Interfaces* **2019**, *11*, 30259.

[47] A. Dobrovolsky, A. Merdasa, E. L. Unger, A. Yartsev, I. G. Scheblykin, *Nat. Commun.* **2017**, *8*, 34.

[48] F. Birch, *Phys. Rev.* **1947**, *71*, 809.

[49] F. Lehmann, A. Franz, D. M. Tobbens, S. Levcenco, T. Unold, A. Taubert, S. Schorr, *RSC Adv.* **2019**, *9*, 11151.

[50] A. L. Montero-Alejo, E. Menéndez-Proupin, D. Hidalgo-Rojas, P. Palacios, P. Wahnón, J. C. Conesa, *J. Phys. Chem. C* **2016**, *120*, 7976.

[51] M. Szafranski, A. Katrusiak, *J. Phys. Chem.* **2016**, *7*, 3458.

[52] S. Jiang, Y. Fang, R. Li, H. Xiao, J. Crowley, C. Wang, T. J. White, W. A. Goddard 3rd, Z. Wang, T. Baikie, J. Fang, *Angew. Chem., Int. Ed.* **2016**, *55*, 6540.

[53] A. Jaffe, Y. Lin, C. M. Beavers, J. Voss, W. L. Mao, H. I. Karunadasa, *ACS Cent. Sci.* **2016**, *2*, 201.

[54] L. Kong, G. Liu, J. Gong, Q. Hu, R. D. Schaller, P. Dera, D. Zhang, Z. Liu, W. Yang, K. Zhu, Y. Tang, C. Wang, S. H. Wei, T. Xu, H. K. Mao, *Proc. Natl. Acad. Sci. USA* **2016**, *113*, 8910.

[55] D. B. Mitzi, *Prog. Inorg. Chem.* **1999**, *48*, 1.

[56] E. S. Parrott, J. B. Patel, A. A. Haghighirad, H. J. Snaith, M. B. Johnston, L. M. Herz, *Nanoscale* **2019**, *11*, 14276.

[57] D. Q. Zhang, L. L. Gu, Q. P. Zhang, Y. J. Lin, D. H. Lien, M. Kam, S. Poddar, E. C. Garnett, A. Javey, Z. Y. Fan, *Nano Lett.* **2019**, *19*, 2850.

[58] M. Anaya, A. Rubino, T. C. Rojas, J. F. Galisteo-López, M. E. Calvo, H. Miguez, *Adv. Opt. Mater.* **2017**, *5*, 1601087.

[59] Q. F. Dong, Y. J. Fang, Y. C. Shao, P. Mulligan, J. Qiu, L. Cao, J. S. Huang, *Science* **2015**, *347*, 967.

[60] D. Shi, V. Adinolfi, R. Comin, M. Yuan, E. Alarousu, A. Buin, Y. Chen, S. Hoogland, A. Rothenberger, K. Katsiev, Y. Losovyj, X. Zhang, P. A. Dowben, O. F. Mohammed, E. H. Sargent, O. M. Bakr, *Science* **2015**, *347*, 519.

[61] M. I. Saidaminov, A. L. Abdelhady, B. Murali, E. Alarousu, V. M. Burlakov, W. Peng, I. Dursun, L. F. Wang, Y. He, G. Maculan, A. Goriely, T. Wu, O. F. Mohammed, O. M. Bakr, *Nat. Commun.* **2015**, *6*, 7586.